Molecular dynamics simulations of liquids and glasses in the system NaAlSiO₄-SiO₂: Methodology and melt structures

Daniel J. Stein, Frank J. Spera

Department of Geological Sciences and Institute for Crustal Studies, University of California,
Santa Barbara, California 93106-9630, U.S.A.

Abstract

This is the first of a two-part molecular dynamics (MD) study that examines the effects of temperature, pressure, and composition on the structure and properties of ten compositions in the system $NaAlSiO_4$-SiO_2. Results were obtained for collections of at least 1300 atoms at temperatures between 2500 and 4500 K, pressures of 2–5 GPa, and simulation durations on the order of 0.1 ns. Durations and numbers of particles are both about three times larger than for previous MD simulations on molten aluminosilicates. This study addresses experimental matters, including aspects of simulation methodology that affect the accuracy of atom trajectories (hence computed properties). These include N_t (total number of atoms in the MD box) and spatial resolution achieved in the interparticle force calculation. Static melt structures and their systematic variation with temperature and composition are also explored. In the second part (Stein and Spera, in preparation), the mechanism of diffusion is studied in detail, and MD-computed results for a variety of thermodynamic and transport properties are reported and related explicitly to melt structure.

The present study employs a pairwise-additive form of the interatomic potential energy function, using the parameters of Dempsey and Kawamura (1984) with electrostatic interactions computed by the Ewald sum technique. Greater than 90% of Si and Al are fourfold-coordinated by O and >90% of O is in twofold coordination by the tetrahedral (T) cations, showing little change with composition and temperature. T-T coordination is found to have a more distinct dependence on composition than does T-O coordination. Structures and properties determined with this set of parameters differ from those computed using the parameters published by Angell et al. (1987), which give a less strongly ordered tetrahedral network and rates of diffusion for network-forming ions that are larger by about an order of magnitude.

Results indicate that transport properties computed from time-correlation functions (e.g., diffusivity and ionic conductivity) apparently become asymptotic for system sizes (N_t) greater than about 1000 particles. Relative to these values, properties computed with N_t less than about 400–600 particles are generally overestimated by 10–100% and show increased variance. Truncation of the Ewald sum (limiting the number of reciprocal space vectors) introduces additional variance in computed properties. Melt structure (e.g., nearest-neighbor coordination statistics, static pair-correlation functions, and intertetrahedral bridging angle distributions) are less dependent upon system size than transport properties. The particular form and parameterization of interionic potential influence computed properties much more than does system size or spatial resolution in the force calculation.

Substitution of (Na + Al) for Si is accompanied by a decrease in the mean intertetrahedral bridging (T-O-T) angle related to increasing numbers of Al-O-Al bridges and produces broader and less sharply peaked angle distributions. Radial density functions computed from the MD configurations reveal muted structure beyond the T-T1 coordination shell in comparison with published XRD analyses, although there is evidence of structure due to T-O2 and T-T2 correlation near 5 Å, especially in the simulation of molten $NaAlSiO_4$. Structures produced by the MD model reflect the effects of using simplistic potential energy functions, as well as characteristically high experiment temperatures and rapid quench rates required by the practical limitations of the MD method.

INTRODUCTION

The ability to extrapolate knowledge of the physical properties of silicate melts and magmas to extreme conditions gives insight into a variety of geophysical and geochemical problems. Of particular concern to geochemists are the properties of glassy or molten silicates relevant to the generation, segregation, ascent, eruption, and crystallization of magma. These phenomena are important in characterizing the origin and evolution of oceanic and continental crust, as well as the parent bodies of the differentiated meteorites, and in understanding the origin and fate of magma oceans, which probably developed during accretion of the Earth and other terrestrial planets (Wetherill, 1990). Solutions to problems in geodynamic transport typically involve analysis of appropriate forms of macroscopic conservation equations. These are unlikely to be meaningful without accurate knowledge of the physical properties of silicate materials. Furthermore, elucidating the relationship between the properties (both static and dynamic) of melts and glasses and their structure at the atomic level facilitates comprehension of a wide variety of complex problems regarding advanced materials of technological importance.

Because of the increasing capability of computers, molecular dynamics (MD) is becoming a cost-effective means of investigating the thermodynamic and transport properties of Earth materials at physical conditions that are difficult or expensive to achieve in the laboratory. An advantage of MD simulations over conventional experiments is the ability to perform many experiments rapidly so that a variety of interaction potentials or a range of parameters for a given form of the potential may be considered. At the same time, the limitations of the MD method should be noted. Specification of the true potential for even simple melts has not been accomplished (Gibbs, 1982; Navrotsky et al., 1985). However, empirical pairwise-additive potentials, which provide for electrostatic (Coulomb) forces and short-range repulsion, and which sometimes include dipole-dipole (van der Waals) interaction, appear to recover the properties of simple molten alkali halides reasonably well (Woodcock, 1975; Sangster and Dixon, 1976). These types of simple central-force potentials similarly enable one to recover the short-range structure and other properties of molten silicates under a range of temperature and pressure conditions. A primary goal of our studies (Stein, 1993; Stein and Spera, in preparation) is to examine the practical capabilities of MD in recovering material properties by making comparisons between simulation and laboratory results. Another goal is to use MD simulations to gain insight into the mechanisms of diffusion, viscous flow, and ionic conductivity. Where appropriate, the MD results are discussed in relation to the intrinsic limitations imposed by use of a simple pairwise-additive potential and by the experimental time scales currently practical for the MD method.

The first applications of MD to silicate compositions reproduced the short-range structure of liquid SiO_2 and binary metal oxide-silica systems (Woodcock et al., 1976; Soules, 1979; Mitra, 1982; Matsui et al., 1982; Matsui and Kawamura, 1984; Erikson and Hostetler, 1987). Since then, the scope of application to problems in physical geochemistry has expanded to include examination of the influence of pressure, temperature, and composition on structure and transport properties (principally ionic self-diffusivity; see, for example, Soules and Busbey, 1981; Angell et al., 1983, 1987; Kubicki and Lasaga, 1988, 1990, 1991; Scamehorn and Angell, 1991). Subsequent efforts have documented the importance of system size (number of particles, N_t) in the determination of high-pressure ionic self-diffusion coefficients (Rustad et al., 1990) and the sensitivity of diffusivity and other properties to variations in the interatomic potentials used in the simulations (Rustad et al., 1991a). As the MD method has been developed, its application in condensed matter physics has employed sophisticated techniques for determining transport properties such as shear viscosity (Ogawa et al., 1990; Wasserman et al., 1993a, 1993b) and thermal conductivity (Lindan and Gillan, 1991).

At temperatures just above the liquidus, substantial structural (volume) reorganization occurs in silicate liquids over time scales on the order of fractions of a microsecond. Measurements of silicate diffusion at 1400–1500 °C (Lesher and Walker, 1986) suggest that network-forming cations may undergo displacements of approximately 1–2 nm over time scales on the order of 10^{-7} s. This average motion is an order of magnitude larger than the average network (T-O) bond length ($\sim$0.16 nm). Structural relaxation mechanisms in near-liquidus silicates are found to occur with frequencies at or just above the MHz range, as indicated by NMR studies of liquid alkali alumino-silicates (Liu et al., 1987, 1988) and also by ultrasonic techniques (Kress et al., 1988, 1989). These relaxation times are greater by a factor of 10^6 than the time scales imposed by MD experiments. The high temperatures used in MD experiments are necessary to make relaxation times small in comparison with the duration of a typical MD experiment. Diffusivities calculated from simulations result in estimated viscosities on the order of 10^{-1} or 10^{-2} Pa·s at a temperature of 3000 K, using the Stokes-Einstein or Eyring relations. Given unrelaxed shear moduli for typical silicate melts ($\sim$25 GPa, see Dingwell and Webb, 1989), a relaxation time of about 10^{-13} s (0.1 ps) characterizes the dynamics at simulation temperatures ($\sim$3500 K). Most of the simulations that this study reports were carried out for durations of 50–100 ps.

Because of the formidable computational requirements of a 1500-particle MD simulation, it is possible to study the computer melt for only a few tenths of a nanosecond of real time. This necessitates simulated cooling rates on the order of 10^4 °C or more per nanosecond (about a billion times greater than the most rapid laboratory quench rates). Because viscosity increases extremely rapidly near the glass transition temperature (T_g), the relaxation time for velocity and stress autocorrelation rises

dramatically and becomes $\gg 10^{-9}$ s. T_g is known to depend on cooling rate and increases with the rate of quenching such that, in the glass transition region, most properties become history- or frequency-dependent (e.g., thermal expansivity, cf. Scherer, 1986; Zarzycki, 1991). Investigations of silicates spanning the liquid-to-glass transition in temperature have, by altering the cooling history, detected changes in the temperature at which thermodynamic equilibrium is lost, arresting the material in a glassy state (e.g., Moynihan et al., 1976). Examination of the phase-space trajectories of MD systems makes it possible to evaluate the point and degree of departure of a simulation from ergodic behavior owing to the extreme quench rates typical of MD simulations (see, for example, Barrat et al., 1990; Barrat and Klein, 1991). This limitation should be kept in mind when determining the range of validity of MD-generated properties. For network silicate systems at high temperature, deviations from Arrhenian behavior remain small, and the activation energy observed for melt viscosity and ionic self-diffusion is nearly temperature independent. This facilitates extrapolation of high-temperature MD results to lower temperature conditions for comparison with laboratory data. One purpose of this study is to examine in detail the breakdown of ergodic behavior with respect to the mobility of Na, Al, Si, and O atoms in simulated sodium aluminosilicate melts (Stein and Spera, in preparation).

Laboratory data are essential to test the ability of the simulations to make valid predictions. The system $NaAlSiO_4$-SiO_2 has been particularly well studied experimentally, especially regarding the relationship of structure to static and dynamic properties. Studies include measurements of physical properties such as density (Riebling, 1966), viscosity (Riebling, 1966; Stein and Spera, 1993, and references therein), glass and crystalline phase spectroscopy (Sharma et al., 1978; Taylor and Brown, 1979a, 1979b; McMillan et al., 1982; Seifert et al., 1982; Mysen et al., 1983), phase equilibria (Greig and Barth, 1938; Schairer and Bowen, 1956), and thermochemical properties (Navrotsky et al., 1982; Richet and Bottinga, 1984). Additional studies include experimental measurements of the viscosity of albite and jadeite melts at high temperatures and pressures (Kushiro, 1976, 1978) and diffusivity of tetrahedral cations and O in jadeite melt (Kushiro, 1983; Shimizu and Kushiro, 1984).

Several previous MD studies exist for sodium aluminosilicate compositions. Dempsey and Kawamura (1984) discussed short- and medium-range melt structure for systems containing about 500 atoms and compared their results to existing X-ray diffraction data. Angell et al. (1983) and Scamehorn and Angell (1991) related structure to patterns of diffusive behavior, particularly at extreme pressures (20–40 GPa). The studies of Angell and coworkers focus on illustrating the concepts of strength and fragility with respect to relaxation mechanisms in liquids (Angell, 1988, 1991); comparison between simulation and laboratory results is not emphasized. These

studies were performed with 400 particles (N_t) for durations on the order of 10^{-11} s (10 ps) and do not report the sensitivity of computed properties to system size or the choice of parameters for computing potential energy. A study of sodium aluminosilicates by Zirl and Garofalini (1990) made use of three-body forces for O-(Si,Al)-O triplets, with $N_t < 400$ atoms per simulation. The present study shows that for properties that require the determination of time-correlation functions (such as self-diffusivity), the roles of the spatial resolution (number of reciprocal lattice vectors used in the Ewald sum calculation) and the size of the MD cell (or total particle number, N_t) must be carefully evaluated.

There has been little work on the sensitivity of MD-computed properties to variations in the parameterization and form of the interionic potential. For this reason, our molecular dynamics study presents results on the structure, thermodynamic, and transport properties in $NaAlSiO_4$-SiO_2, using parameters for the interaction potentials different from those employed by Angell and coworkers and by Rustad et al. (1990, 1991a, 1991b) for SiO_2. It reports results on ten sodium aluminosilicate compositions at simulation temperatures between 2500 and 4000 K and pressures in the range of 2–5 GPa. Properties discussed include short-range structural parameters (radial distribution function or RDF, distribution of intra- and intertetrahedral angles, and coordination statistics for the network cations). Heat capacity, isothermal compressibility, coefficients of self-diffusion of Na, Al, Si, and O ions, and ionic conductivity are addressed in the second part of the study (Stein and Spera, in preparation). The second part also examines the mechanism of the transition from liquid-like to glassy behavior observed in the kinetics of network cations and O. At least for $NaAlSiO_4$-rich compositions in this system, the range of temperature studied here spans the critical temperature at which this transition from ergodic to nonergodic behavior occurs.

Experimental Matters

Molecular dynamics technique

We performed equilibrium molecular dynamics simulations of ten compositions in the system $NaAlSiO_4$-SiO_2 in the microcanonical (NVE) ensemble. In contrast to laboratory experiments, which are inevitably slightly off-composition, the common molar ratio Na/Al = 1 is specified exactly for each simulation. In the molten state at 3–4 GPa pressure, all simulated compositions have structures (see below) in which virtually all O ions occur as bridges between pairs of silicate or aluminate tetrahedra (i.e., O is twofold-coordinated by Si or Al). Densities similar to those measured for the respective glasses under standard conditions of temperature and pressure (in the range 2250–2350 kg/m³) resulted in pressures around 3.5 $\pm$ 1 GPa at the simulation temperatures (2500, 3000, 3500, 4000, and 4500 K). Several simulations in the NPT ensemble were also made in order to compute isothermal compressibilities for comparison with laboratory results.

TABLE 1. Born-Mayer parameters

Pair	A_{ij} (J)		B_{ij} (m^{-1} $\times$ 10^{-9})	
	DK84	SA91	DK84	SA91
Si-O	1.3402 $\times$ 10^{-15}	3.1295 $\times$ 10^{-16}	46.512	34.483
O-O	9.6024 $\times$ 10^{-17}	1.7014 $\times$ 10^{-16}	27.778	34.483
Al-O	1.1251 $\times$ 10^{-15}	3.0914 $\times$ 10^{-16}	45.455	34.483
Na-O	6.2917 $\times$ 10^{-16}	1.6683 $\times$ 10^{-16}	40.000	34.483
Al-Si	9.7093 $\times$ 10^{-10}	3.7906 $\times$ 10^{-16}	133.333	34.483
Na-Si	3.7202 $\times$ 10^{-12}	2.2794 $\times$ 10^{-16}	95.238	34.483
Si-Si	4.7705 $\times$ 10^{-9}	3.6839 $\times$ 10^{-16}	142.857	34.483
Na-Al	1.7710 $\times$ 10^{-12}	2.3094 $\times$ 10^{-16}	90.909	34.483
Al-Al	2.4213 $\times$ 10^{-10}	3.8832 $\times$ 10^{-16}	125.000	34.483
Na-Na	1.1310 $\times$ 10^{-13}	1.3353 $\times$ 10^{-16}	71.429	34.483

Note: sources for parameters are as follows: DK84 = Dempsey and Kawamura (1984); SA91 = Scamehorn and Angell (1991). For interactions involving Si, entries for SA91 correct an error in reporting σ_{Si} by Scamehorn and Angell (1991).

Three of the selected compositions are those of the interior invariant points in the low-pressure phase diagram of the system (cf. Greig and Barth, 1938; Schairer and Bowen, 1956) and have NaAlSiO$_4$-SiO$_2$ ratios near 1:4, 2:3, and 3:2 (labeled N20, N41, and N60, respectively, to indicate mole percent of NaAlSiO$_4$ component). Others include compositions of the mineral phases albite, jadeite, and nepheline (labeled N33, N50, and N100, respectively). These six compositions were simulated polythermally and were the same as those studied in the rheometric laboratory experiments of Stein and Spera (1993). Simulations were also obtained for compositions with NaAlSiO$_4$-SiO$_2$ ratios of 8:7, 4:3, 5:3, and 2:1 (labeled N53, N57, N63, and N66, respectively) at 4000 K only. Most experiments were 40 ps in duration, although some were extended to 70 or 80 ps, and systems contained 1300 $\pm$ 2 particles, depending on stoichiometry. Limited results for simulations of SiO$_2$ are included where appropriate as a point of reference with respect to the numerous MD studies available for that composition.

The computer program for the simulation was based on FORTRAN routines referred to in Allen and Tildesley (1987) and modified and enhanced by Rustad et al. (1990, 1991a). Additional codes to perform correlation-ensemble statistical mechanics and visualization were developed as part of the present study (see also Stein and Spera, in preparation). Simulations were performed on CRAY C90 and CRAY Y-MP systems and on IBM RS/6000-350 workstations. On a CRAY C90, the version of the computer program used in this study required 0.3 CPU-second per time step for a 1300-particle simulation; on the workstations, each time step required about 10 CPU seconds.

A pairwise-additive interparticle potential energy was computed according to

$$U_{ij} = \frac{q_i q_j}{r_{ij}} + A_{ij}\exp(-B_{ij}r_{ij})$$

with full ionic charges q_i and q_j, separated by distance r_{ij}. Repulsion energy representing overlap of electronic charge distribution at small particle separations is parameterized

according to the Born-Mayer form: A_{ij} and B_{ij} are given unique values for each ion pair in the simulation on the basis of empirical ionic size and hardness parameters, which effectively determine the curvature of the potential energy function. Parameters A_{ij} and B_{ij} for the exponential repulsion term were taken from Dempsey and Kawamura (1984) and are reproduced in Table 1, along with values used in previous MD studies of sodium aluminosilicates (Angell et al., 1983, 1987; Scamehorn and Angell, 1991, denoted in the text, tables, and figures as SA91; the parameterization of Dempsey and Kawamura, 1984, is denoted as DK84). Note that in Table 1, calculation of SA91 pair interactions involving Si incorporate correction of a typographical error in reporting the Si size parameter σ_{Si} by Scamehorn and Angell (1991). Interactions for each of the cations coordinated with O in appropriate symmetry are compared graphically in Figure 1a–1c for the parameterizations DK84 and SA91. Differences between the two parameter sets are displayed in the sharpness of the repulsive barrier at short-range, as well as the location of and curvature near the potential energy minimum where electrostatic attraction is significant.

Ewald's summation method was used to compute the long-range Coulomb contribution to force and energy, with $\kappa = 5/L$ (the convergence parameter describing the width of the Gaussian canceling distribution surrounding each ion) for cubic cell dimension L. The reciprocal space portion of the sum was limited to reciprocal lattice vectors $\mathbf{k} = 2\pi n/L^2$ such that $|n|^2 \leq 81$. In addition to the truncation of the Ewald sum in k-space, a cutoff of 0.8 nm was employed in the computation of short-range repulsions. The velocity version of the Verlet algorithm (Allen and Tildesley, 1987) was used to recompute particle positions and velocities after each time step, and periodic boundary conditions were implemented such that the primary MD cell was surrounded by replicate images in simple cubic symmetry to minimize effects owing to the presence of surfaces. Each simulation contained approximately 1300 particles, with density near 2300 kg/m^3, requiring a cell-edge dimension of about 2.6 nm. For comparison, in a simulation with $N_t = 195$ particles, $L \approx 1.4$ nm since $N_t \approx L^3$.

Sensitivity to parameterization of interionic potential

It is instructive to consider the effects of different values of the Born-Mayer repulsion parameters on the melt structures and properties obtained in the simulations. For the purposes of this comparison, coordination statistics have been obtained for NaAlSi$_3$O$_8$ at 4000 K by neighbor counting within the distance of the first minimum of the pair-correlation function (see below). Computations comparing the two parameter sets were performed with 1300 particles and used over 900 reciprocal lattice vectors in the Ewald sum calculation. Considerable differences between the two potentials appear in the coordination volumes of O about Si, O about Al, and of tetrahedral cations about O.

Simulations using SA91 give significantly larger near-neighbor coordination shells with higher average coor-

dination of Si and Al by O and of O by (Si + Al). The DK84 parameters lead to a more nearly tetrahedral fluid with about 94% of Si in fourfold-coordination by O and 6% in fivefold-coordination. In contrast, the SA91 parameters lead to about 70% [4]Si and the remaining 30% [5]Si (Fig. 2a). Consistent variations in Al and O coordination are evident (Fig. 2b and 2c). Angell et al. (1983) and Scamehorn and Angell (1991) presented MD results for three of the compositions investigated here (N33, N50, and N100) using the SA91 parameters for the interionic pair potentials (see Table 1). SA91 incorporates a T-O potential with softer short-range repulsions and a shallower attractive well than DK84 (Fig. 1a and 1b), generating simulation pressures (at similar density) that were slightly lower than those of the present study.

Coordination statistics presented by Angell and coworkers were obtained from constant-pressure simulations at high temperature (see Fig. 4 in Scamehorn and Angell, 1991). These simulations display greater O coordination for Al relative to Si at elevated temperatures and prominent temperature variation in Al coordination. In the simulation of $NaAlSiO_4$ performed by Scamehorn and Angell, significant numbers of [6]Al were observed in a 300 K quenched configuration with a reported fictive temperature of 4000 K (Fig. 5 of that study). Differences between Si and Al coordination are not so pronounced in our constant-volume simulations using SA91. Spectroscopic experiments (Stebbins and Sykes, 1990) have detected only very limited concentrations of Si and Al with coordination greater than four in high-pressure aluminosilicate melts (i.e., in glasses quenched from these melts). The populations of anomalously coordinated O generated from the SA91 parameterization suggest differences in thermal expansivity between the two parameterizations within the low- to moderate-pressure conditions of the simulations.

The differences between the respective structural results of the two parameter sets are matched by significant differences in particle mobility. Although we have not made an extensive study of this matter, results are given for the motion of O in molten $NaAlSi_3O_8$ at 4000 K (Fig. 2d). O mean square displacement (MSD) is approximately 10 times greater with SA91 than in results obtained from DK84. These variations in structural and dynamic properties are the direct outcome of differences among various features of the potential energy surface (Fig. 1a and 1b). The potential well of the DK84 parameterization is deeper for silicate and aluminate clusters compared with that for the SA91 values. Additionally, at a given Si-O separation within the distance of the minimum, DK84 is considerably steeper and hence more strongly repulsive. Both of these aspects lead to a more caged behavior of network ions at a given temperature and pressure, resulting in decreased network mobility.

Effects of system size and spatial resolution of Ewald sum calculation

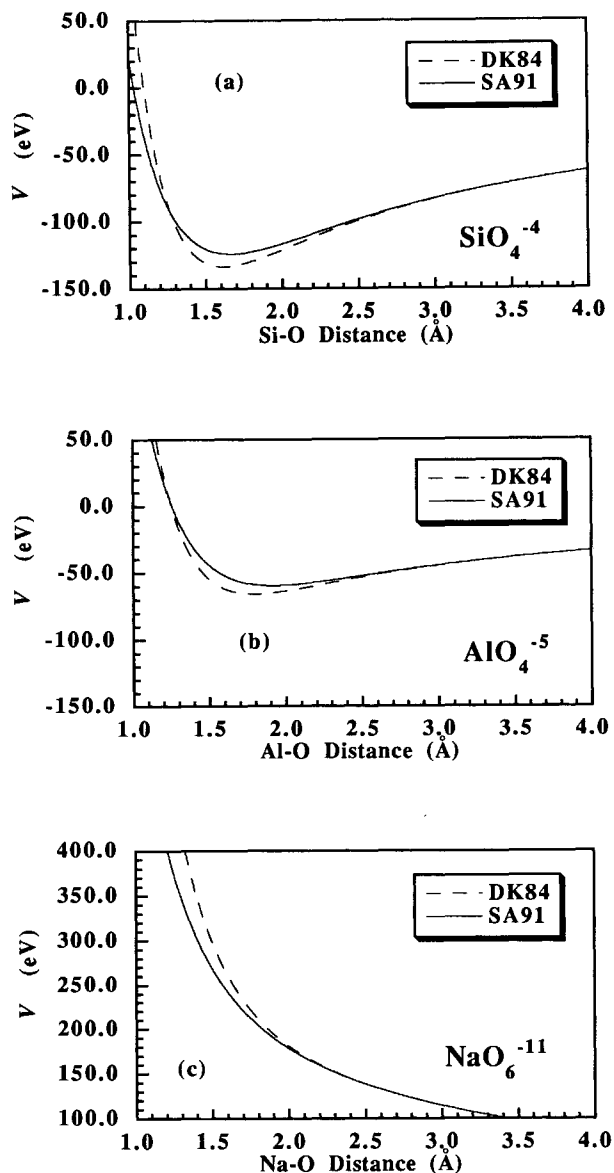A brief study was made of the variation of computed properties with system size (L) or total number of particles

Fig. 1. (a) Potential energy, V, vs. Si-O distance for SiO_4^{-}(tetrahedral symmetry). Vertical axis is energy in electron volts; horizontal axis is Si-O distance in ångströms. Parameters obtained from sources denoted in legend: DK84 = Dempsey and Kawamura (1984); SA91 = Scamehorn and Angell (1991). (b) Same as a for Al-O interaction. (c) Same as a for Na-O (octahedral symmetry).

cles ($N_t \approx L^3$) and the number of reciprocal lattice vectors utilized in the indirect portion of the Ewald sum calculation. Self-diffusivities for Na, Al, Si, and O and a typical static (thermodynamic) property, the isochoric heat capacity, C_v, were considered. One result is that underresolution in space (i.e., too small N_t, L, or $|n|^2$) leads to calculated C_v values that are systematically too high by 10–30%. The effect of poor spatial resolution on self-diffusivities is similar: underresolved simulations tend to
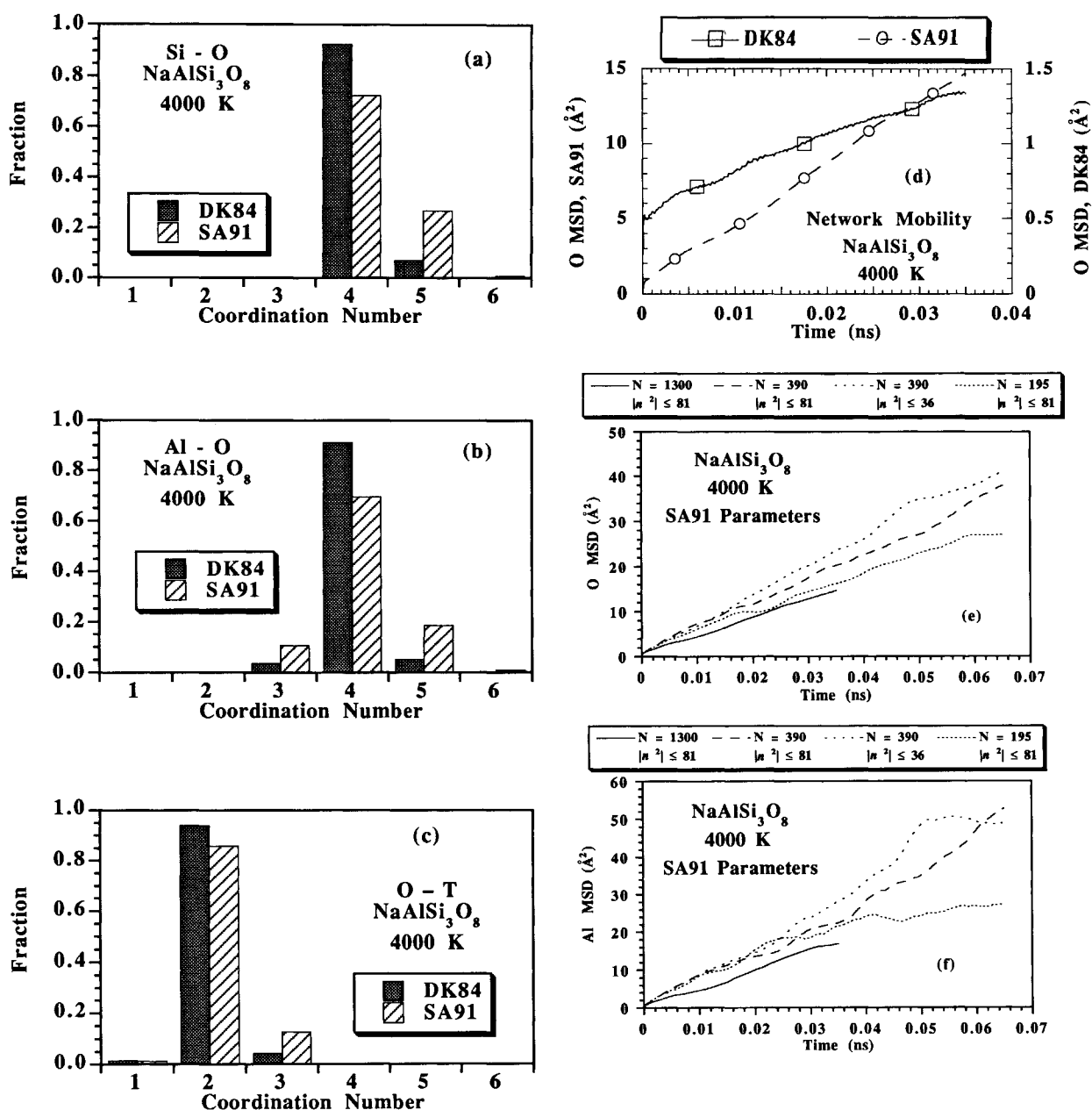
Fig. 2. (a) Comparison of Si-O coordination for $NaAlSi_3O_8$ at 4000 K from simulations using DK84 and SA91 parameters. (b) Same as a but showing Al-O coordination. (c) Same as a but showing coordination of O by nearest-neighbor tetrahedral (T) cations (Si and Al). (d) Effects of choice of potential parameters on O mean square displacement (MSD) for $NaAlSi_3O_8$ at 4000 K. Parameters from sources indicated: DK84 = Dempsey and Kawamura (1984), plotted on right axis; SA91 = Scamehorn and Angell (1991), plotted on left axis. Displacements show differ-

ences of about a factor of 10. Vertical scales are MSD in squared ångströms; horizontal scale is time in nanoseconds. (e) Plot of O mean square displacement for simulations of $NaAlSi_3O_8$ using various system sizes (N) and reciprocal space cutoff ($|n|^2$) for Ewald summation; parameters of SA91 at 4000 K. Reduction of system size or spatial resolution results in overestimation of diffusivity and increased uncertainty in values of D (see text). (f) Same as e for Al ions. Note that variances are larger owing to smaller proportions of Al ions relative to O.

generate estimates of D_i that are too large by 10–100%. In sodium aluminosilicate melts the combination of low mobility and abundance of Al ions results in relatively

large variations of Al MSD as a function of both N_t (or L) and the reciprocal space cutoff. By way of example, Figure 2e and 2f show MSD for O and Al in molten

$NaAlSi_3O_8$ at 4000 K using the SA91 potential parameters (see Table 1) in systems with 195, 390, and 1300 particles and variations in the reciprocal space cutoff for the Ewald sum.

Since D varies directly with MSD, one may note that the effect of using too few particles is that estimates of MD-generated self-diffusivity may vary by as much as 100%. For example, Al diffusivity for $N_t = 390$ and reciprocal space cutoff $|n|^2 \le 36$ or 81 varies from about 1×10^{-5} to 1.5×10^{-5} cm²/s with the less well-resolved case exhibiting greater Al mobility. For more mobile ions or those present in larger numbers, this effect appears smaller but still significant.

Another way to study the effect of system size (L or N_t) on computed transport properties is by analysis of the magnitude of temperature and pressure fluctuations during the production portion of the MD experiment. The magnitude of these fluctuations depends on N_t such that larger fluctuations occur in MD systems of smaller size. Given typical values of the activation energy (E_a) and activation volume (V_a) for self-diffusion, it is possible to recast the temperature and pressure fluctuations during the MD experiment into statistical uncertainties for computed D values. This analysis suggests that σ_D values for O self-diffusion in molten $NaAlSi_3O_8$ at 4000 K and 3 GPa are 3–5 times larger in 195-particle simulations, in comparison with the $N_t = 1300$ experiments employed in the current study.

The fundamental information from any MD simulation is the evolution of location (r_i) and velocity (u_i) of each particle in a specified time interval. Although short-range structure results are relatively insensitive to system size (see below), without adequate phase-space trajectories, dynamic properties will not be accurately determined given, of course, the limitations in the effectiveness of the potential energy functions U_{ij}. The MD study of Rustad et al. (1990) notes that for systems containing small numbers of particles, the particle MSD curves do not converge to a well-defined slope at increasingly long times. Thus the self-diffusion coefficient, which is based on the limiting (infinite time) slope of the MSD curve, cannot be uniquely determined. In effect, the MSD curves are one-dimensional representations of the trajectories computed in the simulations and show that the trajectory computations in small systems are subject to increasing uncertainty with decreasing system size. What is most evident in these comparisons is the increase in size of fluctuations in the rates of ionic diffusivities as spatial resolution (L or reciprocal space cutoff) decreases. These fluctuations necessarily result in greater uncertainty in computed diffusivities, especially when consideration is given to the larger fluctuations of experiment pressure and temperature that occur in systems with smaller N_t. In summary, for a given potential, both system size (L or N_t) and the details of the Ewald summation (specifically, the total number of reciprocal lattice vectors utilized) have a demonstrable effect on the computed material properties. MD primary cells of dimension 25 Å corresponding

to $N_t \approx 1300$ with $|n|^2 \le 81$ recover properties that are at least independent of further increases in spatial resolution. Discrepancies in computed static and transport properties of up to 100% may be incurred in simulations that lack sufficient spatial resolution.

Experimental cooling and equilibration schedule

Random particle positions and a Gaussian velocity distribution appropriate to a temperature of 10000 K were used to begin the computations. The initial steps of the simulation were computed using the repulsion parameters A_{ij} and B_{ij} of SA91 and a time step of 0.1 fs (1 fs = 10^{-15} s); when cell energies became negative, these were replaced by the DK84 parameters and a time step of 1 fs was used throughout the remainder of the simulation. Velocity-scaling methods (Berendsen et al., 1984) were used to bring the system to 10000 K and to change the state of the computer glasses when establishing the final experiment temperatures. Equilibration in the NVE ensemble for 10 ps at 10000 K was followed by velocity-scaled cooling to 3000 K at a rate of 200–300 K/ps. After 20 ps at constant volume and total (potential and kinetic) energy at 3000 K, velocity scaling was again employed to alter the resulting configurations to temperatures near 2500, 3500, or 4000 K where additional NVE trajectories were computed. Total length of NVE simulations for each of the four temperatures was 40 ps, although some experiments were extended to 80 ps in order to develop better statistics. Density was held constant for each composition throughout the simulations; energies remained constant to within one part in 4000; net momenta in the NVE cells were found to be zero to within one part in 10000. For the additional simulations performed at 4000 K (N53, N57, N63, and N66), the NVE experiment durations were 70 ps. For the purposes of obtaining self-diffusion coefficients and structural information, particle positions were saved every 0.05 ps once the target experiment temperature had been attained and stabilized.

RESULTS: SIMULATED MELT STRUCTURES

Once phase-space trajectories (the arrays of positions and velocities saved every 0.05 ps) have been determined, one has the opportunity to determine many correlation functions and hence to recover several static (thermodynamic) and transport properties. For example, application of the Voronoi tessellation (Bernal, 1959, 1960; Bernal and Mason, 1960) and the fluctuation-dissipation theorem (Kubo, 1966) on MD-generated trajectories for the microcanonical (constant NVE) ensemble for silica have been used to correlate high-pressure melt structure with spectral and transport properties (Rustad et al., 1991a, 1991b, 1991c, 1992).

The short-range structural details of the simulation results may be summarized in terms of nearest-neighbor coordination statistics. The potential energy parameters developed by Dempsey and Kawamura (1984) were constrained by their adequacy in reproducing crystal struc-
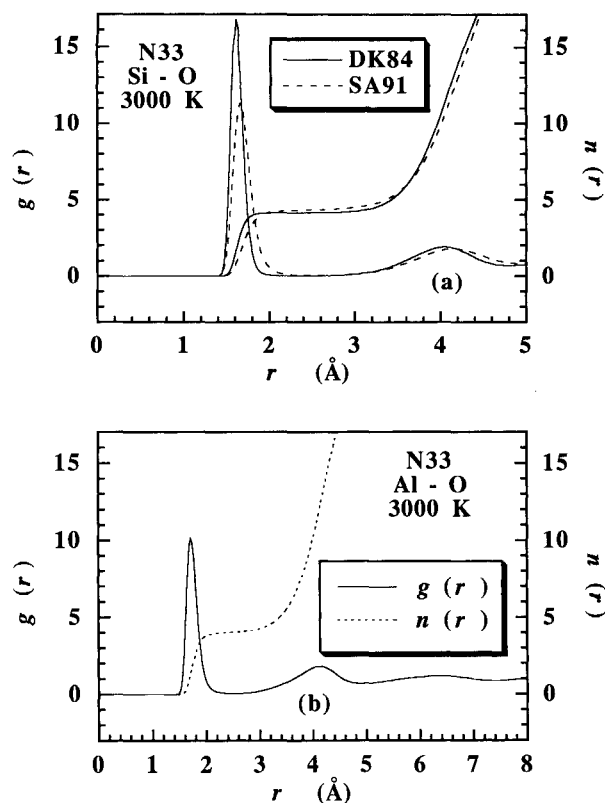
Fig. 3. (a) Pair-correlation function, $g(r)$, and running coordination number, $n(r)$, for the ion pair Si-O in $NaAlSi_3O_8$ at 3000 K, comparing results from DK84 and SA91 parameterizations. The function $n(r)$ was obtained by integration of $g(r)$. Horizontal axis in ångströms; vertical axis for $g(r)$ indicates probability of finding O at various distances from Si relative to overall distribution of O [as r becomes large, function $g(r)$ attains limiting value of unity]; vertical scale for $n(r)$ indicates running average number of O at a specified distance from Si ions. (b) Same as a for pair Al-O, results using DK84 parameters.

tures of sodium aluminosilicate minerals. Soules (1979) and others have noted that structural features reproduced by the MD calculation demonstrate that it is not imperative to employ a model with directional or covalent bonding in order to recover the first-order feature of network silicate fluids—their essentially tetrahedral near-neighbor geometry.

Description of short- and intermediate-range structure in condensed matter simulations generally proceeds from analysis of the pair-correlation function $g(r)$ computed according to standard procedures (see, for example, Allen and Tildesley, 1987). In the present study, features of near-neighbor coordination have been determined by numerical integration of $g(r)$ to obtain $n(r)$ or by counting neighbors within the distance of the first minimum in $g(r)$. Figure 3a shows the relation between $g(r)$ and $n(r)$ for Si-O pairs in the composition $NaAlSi_3O_8$ (N33) at 3000 K and presents results from simulations using both

sets of interaction parameters (DK84 and SA91). The first peak in $g(r)$ is very sharp and, along with the obvious corresponding well-defined plateau of $n(r)$ at just over 4, indicates the high degree of order in the first O coordination sphere around Si. Most O around Si is found within a restricted range of distances, and the first maximum denotes that the most-probable Si-O separation is 0.163 nm. DK84 gives a narrower Si-O distribution than does SA91, generating distinctly smaller average coordination numbers; these evident differences are further addressed below. The Al-O coordination environment is less sharply defined than that for Si-O. Figure 3b presents the $g(r)$ and $n(r)$ functions for the Al-O pair from simulations using DK84; the peak is broader than that for Si-O, and the most probable Al-O separation is 0.171 nm. In the coordination region, values for $n(r)$ are slightly smaller for Al-O than for Si-O. Note that $g(r)$ shows little structure beyond the range of 0.5 to 0.8 nm, which is a function of the high-temperature state and simple form of the potential energy function chosen for the simulations.

Coordination variations with temperature and composition

The difference between the Si-O and Al-O coordination environments is more apparent than are the variation of each respective cation environment with temperature and composition. This distinction between the Si-O and Al-O pairs represents a significant feature of the particle interaction model (DK84) used for these pairs in the simulations, i.e., the Al-O bond is longer and weaker than the Si-O bond. It is this feature that establishes the compositional patterns in various properties computed in the simulations.

For the tetrahedral sites, little variation of $n(r)$ with composition is seen at constant temperature, and even less is seen with temperature at constant composition, although variations are slightly greater for the Al-O pair than for Si-O. Figure 4a illustrates variation of $n(r)$ for the Si-O pair for six compositions at 4000 K. Figure 4b compares $n(r)$ for Si-O in $NaAlSiO_4$ at all temperatures. Figure 4c illustrates the differences in $n(r)$ for Si-O and Al-O pairs in $NaAlSiO_4$ at 2500 and 4000 K; note the greater temperature variation of $n(r)$ for Al-O.

Coordination statistics for the six compositions of Figure 4a were also determined by counting the various nearest-neighbor pairs in a sequence of 800 spatial configurations, each separated in time by 0.05 ps. Table 2 summarizes variations with composition at 4000 K of nearest-neighbor coordination statistics for Si-O, Al-O, and O-T. Spatial variation of average coordination number (Fig. 4a–4c) is obtained from $n(r)$ by integration of $g(r)$ to the distance of its first minimum. O is mostly in fourfold coordination around Si, with the remainder (about 10%) in fivefold coordination, accounting for $n(r)$ values slightly >4 in the 2–3 Å range (Fig. 4a and 4b). O coordination is more variable for Al, with a slightly lower proportion in fourfold coordination than for Si-O, about 5% in fivefold, and the remainder in threefold coor-
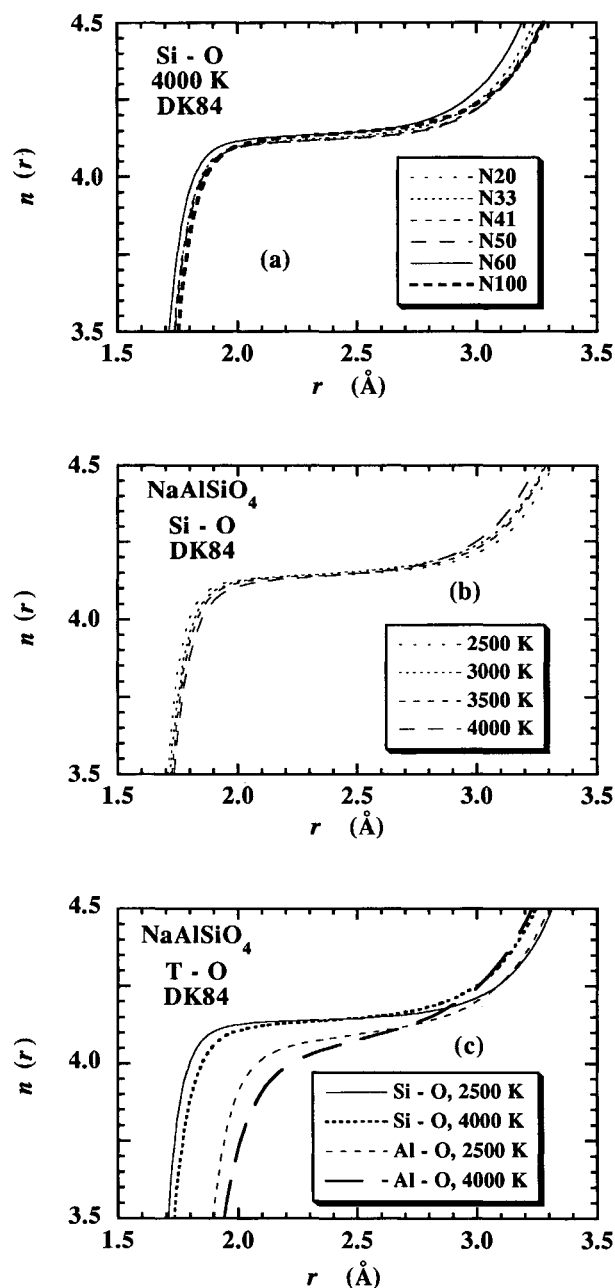
Fig. 4. (a) Plot of running coordination number $n(r)$ for the pair Si-O for selected compositions at 4000 K; note the very muted compositional variation. Horizontal axis in ångströms. The function $n(r)$ was computed by integration of $g(r)$. Simulations used DK84 parameterization. (b) Same as a but showing variations of $n(r)$ with temperature at constant composition (NaAlSiO$_4$). Very little temperature dependence is evident in plateau region. (c) Detail of $n(r)$ for the pairs Si-O and Al-O in NaAlSiO$_4$, comparing results at extremes of temperature. Note that total range on horizontal axis is 2 Å. At a given distance in the coordination shell, Al has lower average coordination than Si.

TABLE 2. Compositional variation of coordination number

CN	N20	N33	N41	N50	N60	N100
			Si-O			
3	0.0	0.0	0.0	0.0	0.022	0.0
4	0.936	0.929	0.934	0.933	0.923	0.908
5	0.064	0.070	0.066	0.067	0.055	0.092
6	<0.001	<0.001	<0.001	<0.001	<0.001	<0.001
			Al-O			
1	0.0	0.0	0.0	0.0	0.005	0.0
2	<0.001	0.0	0.0	0.0	0.005	0.0
3	0.068	0.036	0.042	0.040	0.066	0.024
4	0.888	0.912	0.908	0.917	0.887	0.918
5	0.044	0.051	0.050	0.043	0.035	0.057
6	<0.001	<0.001	<0.001	<0.001	<0.001	<0.001
			O-T			
1	0.011	0.015	0.021	0.018	0.052	0.040
2	0.953	0.941	0.934	0.941	0.892	0.889
3	0.035	0.044	0.045	0.041	0.051	0.070
4	0.0	<0.001	<0.001	<0.001	<0.001	<0.001

Note: coordination number (CN) = fraction of neighboring sites by pair, determined by counting to distance of first minimum in $g(r)$ for all compositions simulated polythermally. O-T refers to coordination of O by combined Si + Al. Results collected at 4000 K.

dination; no obvious trend in composition can be detected. The average O coordination number of Al is actually slightly lower than that for Si, resulting in systematically higher average coordination of O by tetrahedral cations with increasing abundance of Al. Coordination of O by Al + Si is dominantly twofold, and the proportion of twofold O decreases slightly (but systematically) with increasing Al/(Si + Al). As Al/(Si + Al) increases, the slight increase in concentration of more highly-coordinated O that results from mixing of units of NaAlO$_2$ with SiO$_2$ varies consistently with increasing O mobility (Brawer, 1985), decreasing isothermal melt viscosity (Stein and Spera, 1993), and consequent increasing melt fragility (Angell, 1988, 1991). In the constant volume simulations, there is little change in coordination with temperature in the range 2500 K $\leq T \leq$ 4000 K. A consequence of the use of the DK84 parameters is a significantly lower concentration of [3]O compared to the SA91 simulations (Fig. 2c). The fraction of O with only one tetrahedral cation (Si or Al) within the cutoff distance (non-bridging O) necessarily increases with the increase in [3]O. O mobility (Fig. 2d) is a sensitive function of the concentrations of anomalously coordinated O generated depending on choice of parameter scheme.

Considerable order is seen in the T-T coordination environment. Figure 5a shows $g(r)$ for all T—nearest-T pairs for NaAlSi$_2$O$_6$ at 3000 K, including Si-Si, Si-Al, and Al-Al. Compositional ordering of $n(r)$ is similar to that for T-O pairs (Fig. 5b). Figure 5c and 5d show that Al coordination by T is distinctly greater than that of Si by T across the compositional range. This difference between Al and Si coordination is more apparent than in the case of T-O pairs and shows how weakening of the network ordering is amplified in passing from short to intermediate distance scales. This contributes to the explanation of compositional patterns in properties determined by the
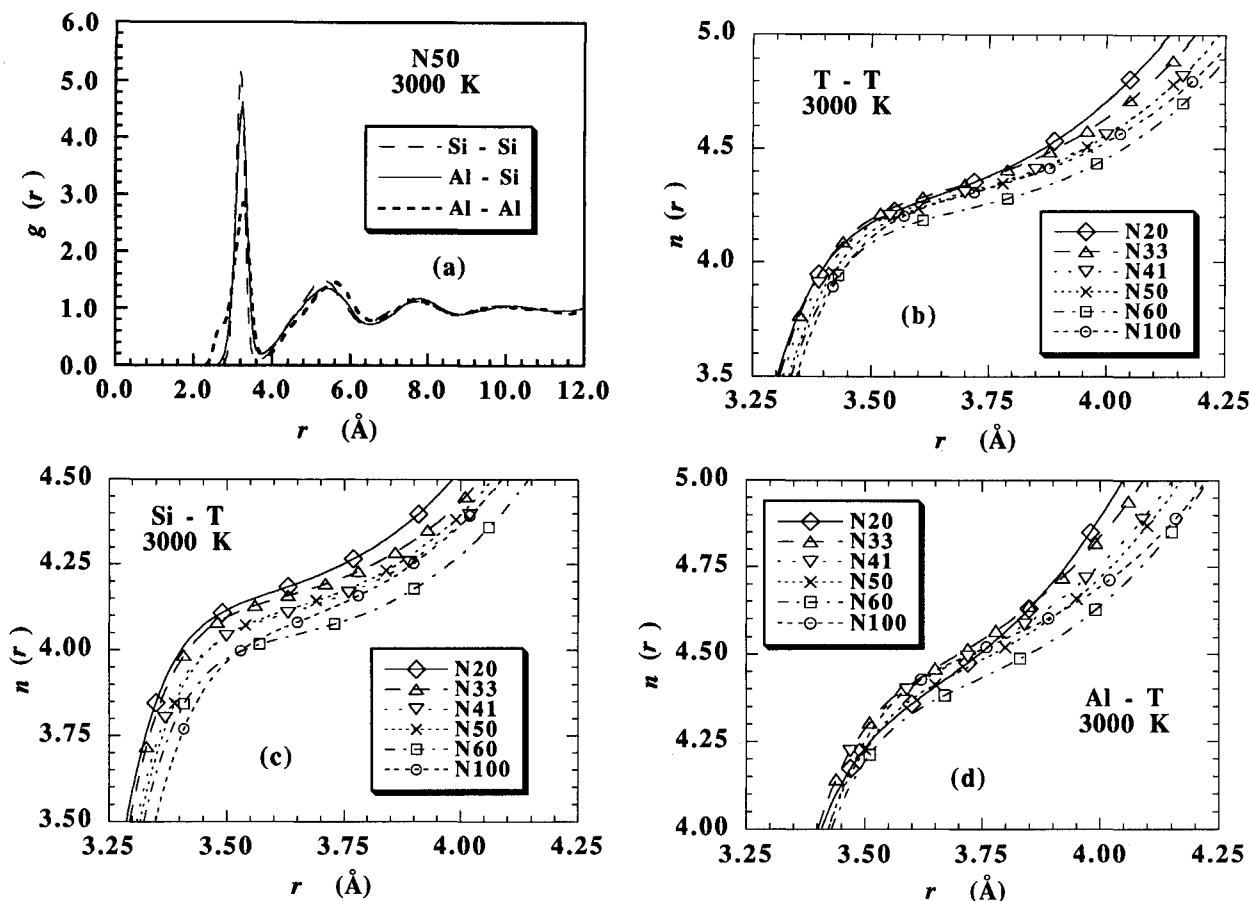
Fig. 5. (a) Pair-correlation function $g(r)$ for Si-Si, Al-Si, and Al-Al pairs in composition $NaAlSi_2O_6$ (N50) at 3000 K; some ordering of T-T pairs persists out to 8 Å. (b) The function $n(r)$ for T-T pairs for all compositions at 3000 K. (c) Same as b for T-T pairs centered on Si. Systematic compositional variation is more evident than for T-O pairs. (d) Same as c for T-T pairs centered on Al. Note that T-T coordination of Al is less ordered than that for Si.

simulations, as well as in laboratory experiments. Indications of systematic compositional variation in non-Arrhenian viscosity behavior in this system have previously been noted (Richet and Bottinga, 1984; Stein and Spera, 1993). Discussion of the concepts of strength and fragility in viscous liquids (Angell, 1988, 1991) relates changes in relaxation mechanisms to patterns in the density of minima on the potential energy surface. Figure 5c and 5d, in illustrating the significant differences of Si-T and Al-T ordering, suggest that increases in the density of minima are contributed by Al sites in the network.

Conspicuously absent from the present series of simulations is the double peak in $g(r)$ for Al-Al that was noted by Dempsey and Kawamura (1984), as well as by Scamehorn and Angell (1991), and attributed to irregular Al polyhedra sharing edges with Al-centered O tetrahedra. We are currently unable to account for this discrepancy, but it is not the result of using small numbers of particles, nor is it simply explained in terms of details of the Ewald sum calculation, because, the double peak does not appear in our results using $N_t = 390$ or in simulations

using lower reciprocal space resolution, regardless of parameterization of repulsions.

Bridging angle distributions

Tetrahedral structural members may be treated more or less as units, and changes in silicate structure and properties are commonly expressed in terms of Si-O-Si (more generally, of intertetrahedral or T-O-T) angle variations or of the fraction of nonbridging O. Of additional interest are properties of the nontetrahedral polyhedra, well documented in crystalline silicates (e.g., Hazen and Finger, 1982) and more recently in glasses as well (Richet et al., 1993). The conventional definition of a bridging O as the O connecting two neighboring (Si,Al)-centered tetrahedra is used. Features of the distribution of intertetrahedral angles are a direct result of the packing geometry of the various (spherical) ions, modified by ongoing diffusive events. However, as has been noted in numerous other studies, the failure to include covalency or directionality in the bonding model causes the average angle to be about 8° too large in comparison with results from spectroscopy

(Taylor and Brown, 1979b; Okuno and Marumo, 1982).

Any melt property that can be related to T-O bond strength will be affected by changes in the intertetrahedral angle (and vice versa). Increasing T-O bond length is associated with decreasing T-O-T angle (Brown et al., 1969). This relationship is particularly well illustrated in the results of the calculation of potential energy surfaces as a function of bond angle and bond distance (Gibbs et al., 1981; Chakoumakos et al., 1981). These studies show that the minimum in potential energy follows a broad trend in which increasing bond angle is correlated with decreasing bond distance. For example, activation energies of diffusion, conductivity, and viscous flow are correlated with the strength of T-O bonds (e.g., de Jong and Brown, 1980a, 1980b). Thus, a lowering of the intertetrahedral angle is associated with enhanced network mobility (increases in diffusivity and ionic conductivity and decreases in viscosity). In crystalline materials of fixed degree of polymerization, as are the compositions in the present study in which all O is nominally bridging, changes in T-O bond length and T-O-T bond angle are interrelated (Gibbs et al., 1972; Brown et al., 1969). As is shown by our results, this aspect of silicate melt structure is well reproduced in the simulations.

The intratetrahedral O-T-O angle distributions for N33, N50, and N100 at 300 K are given in Figure 6a, and the distributions of intertetrahedral bridging (T-O-T) angles at 3000 K obtained for these same compositions are presented in Figure 6b. At low temperature, the O-T-O angle distributions show little variation with composition. The average O-T-O angle is 108.9° for $NaAlSi_3O_8$ and $NaAlSi_2O_6$ and 109.0° for $NaAlSiO_4$ (the normal interior tetrahedral angle is 109.5°). The distributions generally have a standard deviation of about 8 or 9 ° and are slightly positive-skew. Statistics were collected on 400 configurations, each separated by 0.05 ps. Some of the width the T-O-T distributions should be attributed to the fact that ionic mobility precludes computation of angles on the basis of average particle positions, as has been done in simulations of glass structure at lower temperatures. In the case of the O-T-O distribution, it is evident that rapid quenching in MD simulations preserves the characteristics of higher temperature configurations.

The principal features of the bridging (T-O-T) angle statistics revealed by the simulations consist of a general broadening of the peak of the skew-symmetric distributions (increased standard deviation) with increasing Al/ (Si + Al), a trend that is accompanied by a gradual increase in area of the low-angle tail of the distribution. At a representative temperature of 3000 K, the average angle of the distributions decreases by over 5° as composition changes from N20 to N100, as summarized in Table 3. The relation of these patterns to the increasing content of Al in the network cation positions will be discussed in a subsequent section. In Table 3, the statistics of T-O-T angles are further broken down in terms of Si-O-Si, Si-O-Al, and Al-O-Al angles, and the standard deviation also shows systematic compositional behavior, which is
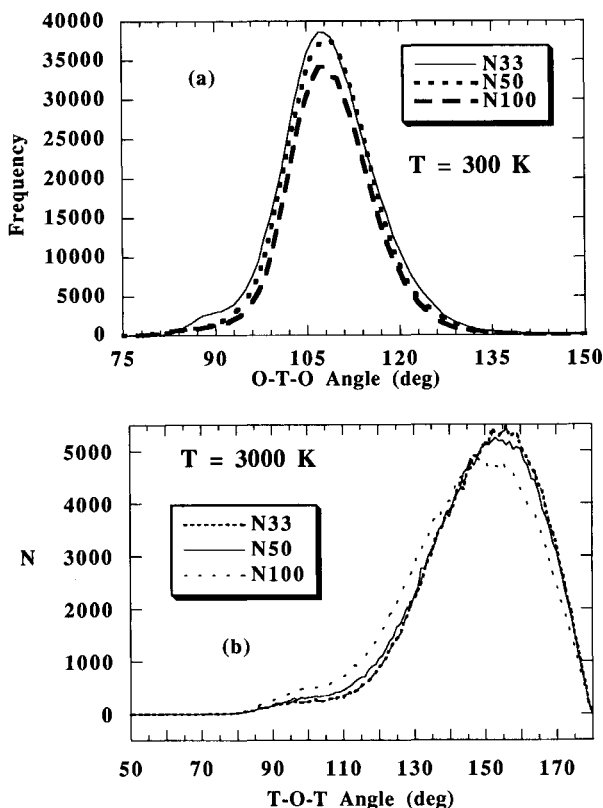

Fig. 6. (a) Distribution of intratetrahedral (O-T-O) angles for $NaAlSi_3O_8$ (N33), $NaAlSi_2O_6$ (N50), and $NaAlSiO_4$ (N100) at 300 K. Average is 108.9° and standard deviation is 8°; geometric intratetrahedral angle is 109.5°. (b) Distribution of intertetrahedral bridging (T-O-T) angles for composition $NaAlSi_3O_8$ (N33), $NaAlSi_2O_6$ (N50), and $NaAlSiO_4$ (N100) at 3000 K. Averages and standard deviations of distributions are given in Table 3.

linked to the compositional variation in T-T neighbor distances (Fig. 5b). Dempsey and Kawamura (1984) noted from examination of the population of Al-O-Al angles in their MD simulations that the Al-avoidance principle is not obeyed in these simulations. We confirm that the distribution of Al-Al neighbors in the simulations is statistically random.

In the simulations performed for the present study, the low T-O-T angle population is correlated with larger T-O and T-T distances, which in turn are correlated with Si or Al sites having larger average coordination numbers. Scamehorn and Angell (1991) presented results showing that the small-angle portion of the distributions contained a much larger proportion of the angles; this is consistent with the differences in their results for average coordination number. However, in examining the $g(r)$ results of Scamehorn and Angell (1991) and Angell et al. (1983), it is not possible to determine if the correlation extends to T-O distance. It may be speculated that these differences are related to the broader, shallower T-O potential well of SA91, permitting significantly greater breakdown of T-O and, hence, T-T order than does the

TABLE 3. Intertetrahedral bridging angles (3000 K)

	Angle	N	Av.	s.d.
SiO₂	Total	208 776	153.163	13.442
N20	Total	211 221	150.62	15.996
	Al-O-Al	4 076	128.02	24.653
	Si-O-Al	64 113	144.97	17.660
	Si-O-Si	143 032	153.80	13.474
N33	Total	213 404	149.35	16.470
	Al-O-Al	11 842	129.22	23.115
	Si-O-Al	86 031	146.59	16.387
	Si-O-Si	115 531	153.46	13.500
N41	Total	214 431	148.98	16.826
	Al-O-Al	15 072	129.15	22.249
	Si-O-Al	95 852	146.33	16.364
	Si-O-Si	103 507	154.32	13.195
N50	Total	214 085	148.39	17.038
	Al-O-Al	21 464	135.39	21.473
	Si-O-Al	104 872	146.34	16.794
	Si-O-Si	87 749	154.02	13.402
N60	Total	209 711	146.81	17.439
	Al-O-Al	29 328	133.07	21.008
	Si-O-Al	104 206	146.29	16.280
	Si-O-Si	76 177	152.79	13.942
N100	Total	217 001	145.14	18.330
	Al-O-Al	50 172	133.31	20.587
	Si-O-Al	120 618	146.71	16.274
	Si-O-Si	46 211	153.92	13.799

Note: angles computed on all T-O-T triplets for T-O distances <2.5 Å; based on about 300 configurations each separated in time by 0.05 ps.

potential of Dempsey and Kawamura (1984) (see Fig. 1). Comparison with laboratory data awaits the results from more definitive spectroscopic studies on these compositions.

Discussion

Recent comments in the literature (Wright, 1993) have noted the inability of the simple potentials used in MD simulations to reproduce the detailed structure of laboratory glasses much beyond the range of the first coordination shell. Furthermore, as noted above, the lack of covalence in the bonding model used in these simulations generated average Si-O-Si angles somewhat larger than those found in actual glasses. Figure 7a–7c compares the radial distribution functions for $NaAlSi_3O_8$ (N33), $NaAlSi_2O_6$ (N50), and $NaAlSiO_4$ (N100) obtained from the MD results with a radial distribution analysis of $NaAlSi_3O_8$ and $NaAlSi_2O_6$ glasses quenched from high pressure (Hochella and Brown, 1985) and $NaAlSiO_4$ glass quenched at low pressure (Aoki et al., 1986). The relative positions of the peaks may be compared, but the intensity scale should be regarded as arbitrary (simulated RDFs have been scaled to match the intensities of the T-O peak and are computed without reference to an actual electron density corresponding to the distribution of nuclei resulting from the MD simulation). The low intensity shoulder at 2.6 Å was interpreted by Hochella and Brown to be due to nearest-neighbor O atoms (those sharing a single T site); this is the location of the first peak of $g(r)$ for O-O in the simulations. In their experiments, considerable reduction in intensity of this peak at higher pressures was attributed to a more diverse set of O-O coordination environments. This peak is relatively prominent

in the simulation results and indicates that the potential energy functions preserve significant O-O correlation at a single T site. Little change with moderate pressure increases is expected in the O-T-O angle distribution (Fig. 6a) in simulations using the DK84 parameters in comparison with SA91. The absence of the prominent RDF peaks beyond about 3.5 Å indicates that such structure is not well defined in the simulations. A peak at 5.0 Å was attributed by Taylor and Brown (1979a, 1979b) to tetrahedral cation separations on opposite sides of rings consisting of six tetrahedra but is not evident in the simulation results. The high-temperature structural state contributes to the damping of intermediate range order.

The simple form of ionic pair potential energy functions used in these simulations adequately reproduces the average nearest-neighbor coordination tetrahedral structure of these fully polymerized melts. Coordination statistics also show a significant population of [5]Si (5–10%) as well as [3]O (4–7%) and 2–5% nonbriding O sites (Fig. 2a–2c). Spectroscopic studies have detected similar concentrations of anomalously coordinated species in glasses quenched from melts at pressures up to 10 GPa, but only in significantly depolymerized alkali silicate compositions. Spectroscopic results on $NaAlSi_3O_8$ (Stebbins and Sykes, 1990) have measured barely detectable quantities of these anomalously coordinated species. The reason for the discrepancy as well as the generally high degree of medium range disorder (e.g., in the angle distributions) is that our coordination statistics were collected in a dynamic system capable of recording diffusive events (or similar vibrational states that do not relax by diffusion), whereas the high-pressure glasses were examined spectroscopically at low temperatures in a static (i.e., frozen) state.

The diffusion rates of network forming species in these simulated melts are controlled by the motions of several ions around a defect site (cf. Brawer, 1985; Kubicki and Lasaga, 1988) and are thus sensitive to intermediate-range structure. Aspects of these diffusive events are discussed in detail in the second part of this study. Insofar as the bonding model is pairwise-additive, the intent of the simulation is not to mimic faithfully the energetics of site exchange in diffusive events that involve the cooperative motions of several particles. The details of such processes must be left to future quantum mechanical studies of clusters of atoms and MD simulations that incorporate multi-body forces. In any event, there is a difference in the ionicity of the Al-O and Si-O bonds, and changes in the bonding character of the tetrahedral silicate structure with temperature and pressure, which have been discussed in other studies, may find compositional analogies in this system. MD simulations of sodium aluminate currently in progress may provide additional insight into this problem.

Conclusions

Results obtained in the present study demonstrate that dynamic properties such as self-diffusivity determined by

MD simulation are strongly influenced by choice of parameterization and, to a lesser extent, by system size and spatial resolution incorporated in details of the Ewald sum calculation. Order of magnitude differences in transport behavior result from different parameterization of the interionic repulsions, while differences of 10–100% in material properties (static and transport) may result from changes in system size and spatial resolution. Use of increasingly larger numbers of particles appears to lead to stabilization of transport values at a lower bound. Structural details are less sensitive to system size than properties determined from time-correlation functions. Progressive changes in structure are observed by substituting Na + Al for Si in a continuous aluminosilicate network, and the choice of parameterization of the interparticle potential affects both structural features and particle mobilities in an internally consistent manner.

In the results reported here, patterns in coordination statistics reveal weak compositional variation of the tetrahedral (near-neighbor) structures. Stronger patterns are seen in the second neighbor (e.g., T-T coordination, Fig. 5, and intra- and intertetrahedral angle distributions, Fig. 6). T-T coordination number systematically increases in the compositional series from N20 to N100. In the same compositional series, the distributions of intertetrahedral (T-O-T) angles broaden and become less sharply peaked, with growth in the low-angle tail. The average angle decreases and the standard deviation increases systematically. This is a function of a less ordered coordination environment around the Al sites (related to the density of local minima on the potential energy surface), which increase in concentration as $NaAlO_2$ is added to molten silica.

A significant detail of the bonding model used in the present study is the longer and weaker Al-O bond relative to Si-O. As Na + Al replaces Si in the silicate network, average coordination of O by tetrahedral cations and coordination of Si and Al by their nearest tetrahedral cation neighbors increase systematically. A similar compositional trend holds true for the intertetrahedral bridging (T-O-T) angle distributions, which become broader and skewed toward smaller angles, related to the increasing population of Al-O-Al bridges. Structural results have also been compared to available X-ray diffraction measurements of radial distribution functions obtained for $NaAlSi_3O_8$, $NaAlSi_2O_6$, and $NaAlSiO_4$ compositions. Structural information obtained in this study also reflects the effects of the high simulation temperatures and the rapid quench rates of the simulations. These conditions are imposed by limitations in computational resources in order to observe dynamic properties (e.g., self-diffusivity) sensitive to melt structural relaxation times. In a companion study (Stein and Spera, in preparation), these results are related to compositional and temperature variations in thermodynamic and transport properties obtained in the simulations. The range of composition, temperature, and simulation duration spanned in the present study is sufficient to encompass the melt-to-glass transition with respect to ion mobilities.
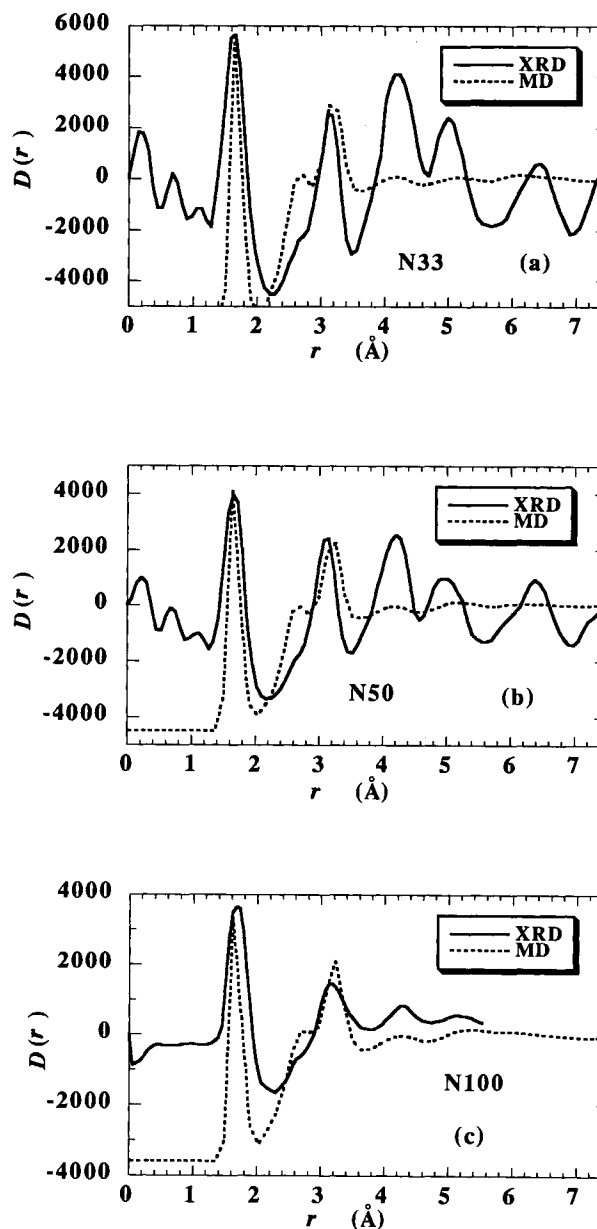

Fig. 7. (a) Comparison of radial density functions computed from simulation results for $NaAlSi_3O_8$ (N33) at 3000 K with those measured in X-ray diffraction experiments of Hochella and Brown (1985). Radial density is defined by $D_{ij}(r) = 4\pi r^2 [\rho(r) - \rho_0]$, where $\rho(r)$ is the number density of species j with respect to species i evaluated at any r, and ρ_0 is the average number density of species j with respect to species i. MD indicates simulation result; XRD indicates result from X-ray diffraction measurements. $D(r)$ from simulations computed from sums of individual pair correlations and normalized to match T-O peak (near 1.6 Å) intensity measured in X-ray diffraction (XRD) studies. Peak near 3.2 Å is due to T-T correlations; peak between 4 and 4.5 Å is attributed to T–second O and that around 5 Å is attributed to T–second-nearest T neighbors (see Fig. 5a). (b) Same as a for $NaAlSi_2O_6$ (N50). XRD results from Hochella and Brown (1985). (c) Same as a for $NaAlSiO_4$ (N100). XRD results from Aoki et al. (1986).

References cited

Allen, M.P., and Tildesley, D.J. (1987) Computer simulation of liquids, 385 p. Oxford University Press, New York.

Angell, C.A. (1988) Perspective on the glass transition. Journal of Physics and Chemistry of Solids, 49, 863–871.

——— (1991) Relaxation in liquids, polymers and plastic crystals: Strong/fragile patterns and problems. Journal of Non-Crystalline Solids, 131, 13–31.

Angell, C.A., Cheeseman, P., and Tamaddon, S. (1983) Water-like transport property anomalies in liquid silicates investigated at high T and P by computer simulation techniques. Bulletin de Minéralogie, 106, 87–97.

Angell, C.A., Cheeseman, P.A., and Kadiyala, R.R. (1987) Diffusivity and thermodynamic properties of diopside and jadeite melts by computer simulation studies. Chemical Geology, 62, 83–92.

Aoki, N., Yambe, S., Inoue, H., Hasegawa, H., and Yasui, I. (1986) An X-ray diffraction study of the structure of Na_2O, Al_2O_3, $2SiO_2$ glass. Physics and Chemistry of Glasses, 27, 124–127.

Barrat, J.-L., and Klein, M.L. (1991) Molecular dynamics simulations of supercooled liquids near the glass transition. Annual Review of Physical Chemistry, 42, 23–53.

Barrat, J.-L., Roux, J.-N., and Hansen, J.-P. (1990) Diffusion, viscosity and structural slowing down in soft sphere alloys near the kinetic glass transition. Chemical Physics, 149, 197–208.

Berendsen, H.J.C., Postma, J.P.M., van Gunsteren, W.F., DiNola, A., and Haak, J.R. (1984) Molecular dynamics with coupling to an external bath. Journal of Chemical Physics, 81, 3684–3690.

Bernal, J.D. (1959) A geometrical approach to the structure of liquids. Nature, 183, 141–147.

——— (1960) Geometry of the structure of monatomic liquids. Nature, 185, 68–70.

Bernal, J.D., and Mason, J. (1960) Co-ordination of randomly packed spheres. Nature, 188, 910–911.

Brawer, S. (1985) Relaxation in viscous liquids and glasses, 220 p. American Ceramic Society, Columbus.

Brown, G.E., Gibbs, G.V., and Ribbe, P.H. (1969) The nature and variation in length of the Si-O and Al-O bonds in framework silicates. American Mineralogist, 54, 1044–1061.

Chakoumakos, B.C., Hill, R.J., and Gibbs, G.V. (1981) A molecular orbital study of rings in silicates and siloxanes. American Mineralogist, 66, 1237–1249.

de Jong, B.H.W.S., and Brown, G.E. (1980a) Polymerization of silicate and aluminate tetrahedra in glasses, melts, and aqueous solutions: I. Electronic structure of $H_6Si_2O_7$, $H_6AlSiO_7^{1-}$, and $H_6Al_2O_7^{2-}$. Geochimica et Cosmochimica Acta, 44, 491–511.

——— (1980b) Polymerization of silicate and aluminate tetrahedra in glasses, melts, and aqueous solutions: II. The network modifying effects of Mg^{2+}, K^+, Na^+, Li^+, H^+, OH^-, F^-, Cl^-, H_2O, CO_2 and H_3O^+ on silicate polymers. Geochimica et Cosmochimica Acta, 44, 1627–1642.

Dempsey, M.J., and Kawamura, K. (1984) Molecular dynamics simulation of the structure of aluminosilicate melts. In C.M.B. Henderson, Ed., Progress in experimental petrology, p. 49–56. Natural Environment Research Council, Manchester, U.K.

Dingwell, D.B., and Webb, S.L. (1989) Structural relaxation in silicate melts and non-Newtonian melt rheology in geologic processes. Physics and Chemistry of Minerals, 16, 508–516.

Erikson, R.L., and Hostetler, C.J. (1987) Application of empirical ionic models to SiO_2 liquid: Potential model approximations and integration of SiO_2 polymorph data. Geochimica et Cosmochimica Acta, 51, 1209–1218.

Gibbs, G.V. (1982) Molecules as models for bonding in silicates. American Mineralogist, 67, 421–450.

Gibbs, G.V., Hamil, M.M., Louisnathan, S.J., Bartell, L.S., and Yow, H. (1972) Correlations between Si-O bond length, Si-O-Si bond angle and bond overlap populations calculated using extended Hückel molecular orbital theory. American Mineralogist, 57, 1578–1613.

Gibbs, G.V., Meagher, E.P., Newton, M.D., and Swanson, D.K. (1981) Comparison of experimental and theoretical bond length and angle variations for minerals and inorganic solids and molecules. In M. O'Keeffe and A. Navrotsky, Eds., Structure and bonding in crystals, p. 195–225. Academic, New York.

Greig, J.W., and Barth, T.F.W. (1938) The system $Na_2O \cdot Al_2O_3 \cdot 2SiO_2$ (nephelite, carnegieite)-$Na_2O \cdot Al_2O_3 \cdot 6SiO_2$ (Albite). American Journal of Science (5th Series), 35A, 93–112.

Hazen, R.M., and Finger, L.W. (1982) Comparative crystal chemistry, 231 p. Wiley, New York.

Hochella, M.F., and Brown, G.E. (1985) The structures of albite and jadeite composition glasses quenched from high pressure. Geochimica et Cosmochimica Acta, 49, 1137–1142.

Kress, V.C., Williams, Q., and Carmichael, I.S.E. (1988) Ultrasonic investigation of melts in the system Na_2O-Al_2O_3-SiO_2. Geochimica et Cosmochimica Acta, 52, 283–293.

——— (1989) When is a silicate melt not a liquid? Geochimica et Cosmochimica Acta, 53, 1687–1692.

Kubicki, J.D., and Lasaga, A.C. (1988) Molecular dynamics simulations of SiO_2 melt and glass: Ionic and covalent models. American Mineralogist, 73, 941–955.

——— (1990) Molecular dynamics and diffusion in silicate melts. In J. Ganguly, Ed., Diffusion, atomic ordering, and mass transport: Selected problems in geochemistry, p. 1–50. Springer-Verlag, New York.

——— (1991) Molecular dynamics simulations of pressure and temperature effects on $MgSiO_3$ and Mg_2SiO_4 melts and glasses. Physics and Chemistry of Minerals, 17, 661–673.

Kubo, R. (1966) The fluctuation dissipation theorem. Reports of Progress in Physics, 29, 255–284.

Kushiro, I. (1976) Changes in viscosity and structure of melt of $NaAlSi_2O_6$ composition at high pressures. Journal of Geophysical Research, 81, 6347–6350.

——— (1978) Viscosity and structural changes of albite ($NaAlSi_3O_8$) melt at high pressures. Earth and Planetary Science Letters, 41, 87–90.

——— (1983) Effect of pressure on the diffusivity of network-forming cations in melts of jadeitic compositions. Geochimica et Cosmochimica Acta, 47, 1415–1422.

Lesher, C.E., and Walker, D. (1986) Solution properties of silicate liquids from thermal diffusion experiments. Geochimica et Cosmochimica Acta, 50, 1397–1411.

Lindan, P.J.D., and Gillan, M.J. (1991) A molecular dynamics study of the thermal conductivity of CaF_2 and UO_2. Journal of Physics: Condensed Matter, 3, 3929–3939.

Liu, S.B., Pines, A., Brandriss, M., and Stebbins, J.F. (1987) Relaxation mechanisms and effects of motion in albite ($NaAlSi_3O_8$) liquid and glass: A high temperature NMR study. Physics and Chemistry of Minerals, 15, 155–162.

Liu, S.-B., Stebbins, J.F., Schneider, E., and Pines, A. (1988) Diffusive motion in alkali silicate melts: An NMR study at high temperature. Geochimica et Cosmochimica Acta, 52, 527–538.

Matsui, Y., and Kawamura, K. (1984) Computer simulation of structures of silicate melts and glasses. In I. Sunagawa, Ed., Materials science of the Earth's interior, p. 3–23. Reidel, Boston.

Matsui, Y., Kawamura, K., and Syono, Y. (1982) Molecular dynamics calculations applied to silicate systems: Molten and vitreous $MgSiO_3$ and Mg_2SiO_4 under low and high pressures. In S.-I. Akimoto and M.H. Manghnani, Eds., High pressure research in geophysics, p. 511–524. Reidel, Boston.

McMillan, P., Piriou, B., and Navrotsky, A. (1982) A Raman spectroscopic study of glasses along the joins silica-calcium aluminate, silica-sodium aluminate, and silica-potassium aluminate. Geochimica et Cosmochimica Acta, 46, 2021–2037.

Mitra, S.K. (1982) Molecular dynamics simulation of silicon dioxide glass. Philosophical Magazine, 45B, 529–548.

Moynihan, C.T., Easteal, A.J., DeBolt, M.A., and Tucker, J. (1976) Dependence of fictive temperature of glass on cooling rate. Journal of the American Ceramic Society, 59, 12–16.

Mysen, B.O., Virgo, D., Danckwerth, P., Seifert, F.A., and Kushiro, I. (1983) Influence of pressure on the structure of melts on the joins $NaAlO_2$-SiO_2, $CaAl_2O_4$-SiO_2, and $MgAl_2O_4$-SiO_2. Neues Jahrbuch für Mineralogie Abhandlungen, 147, 281–303.

Navrotsky, A., Peraudeau, G., McMillan, P., and Coutures, J.-P. (1982) A thermochemical study of glasses and crystals along the joins silica-calcium aluminate and silica-sodium aluminate. Geochimica et Cosmochimica Acta, 46, 2039–2047.

Navrotsky, A., Geisinger, K.L., McMillan, P., and Gibbs, G.V. (1985) The tetrahedral framework in glasses and melts: Inferences from molecular orbital calculations and implications for structure, thermodynamics, and physical properties. Physics and Chemistry of Minerals, 11, 284–298.

Ogawa, H., Shiraishi, Y., Kawamura, K., and Yokokawa, T. (1990) Molecular dynamics study on the shear viscosity of molten Na_2O-$2SiO_2$. Journal of Non-Crystalline Solids, 119, 151–158.

Okuno, M., and Marumo, F. (1982) The structures of anorthite and albite melts. Mineralogical Journal, 11, 180–196.

Richet, P., and Bottinga, Y. (1984) Glass transitions and thermodynamic properties of amorphous SiO_2, $NaAlSi_nO_{2n+2}$ and $KAlSi_3O_8$. Geochimica et Cosmochimica Acta, 48, 453–470.

Richet, P., Robie, R.A., and Hemingway, B.S. (1993) Entropy and structure of silicate melts. Geochimica et Cosmochimica Acta, 57, 2751–2766.

Riebling, E.F. (1966) Structure of sodium aluminosilicate melts containing at least 50 mole % SiO_2 at 1500 °C. Journal of Chemical Physics, 44, 2857–2865.

Rustad, J.R., Yuen, D.A., and Spera, F.J. (1990) Molecular dynamics of liquid SiO_2 under high pressure. Physical Review A, 42, 2081–2089.

——— (1991a) The sensitivity of physical and spectral properties of silica glass to variations of interatomic potentials under high pressure. Physics of the Earth and Planetary Interiors, 65, 210–230.

——— (1991b) Molecular dynamics of amorphous silica at very high pressures (135 GPa): Thermodynamics and extraction of structures through analysis of Voronoi polyhedra. Physical Review B, 44, 2108–2121.

——— (1991c) The statistical geometry of amorphous silica at lower mantle pressures: Implications for melting slopes of silicates and anharmonicity. Journal of Geophysical Research, 96, 19665–19673.

——— (1992) Coordination variability and the structural components of silica glass under high pressures. Chemical Geology, 96, 421–437.

Sangster, M.J.L., and Dixon, M. (1976) Interionic potentials in alkali halides and their use in simulations of the molten salts. Advances in Physics, 25, 247–342.

Scamehorn, C.A., and Angell, C.A. (1991) Viscosity-temperature relations and structure in fully polymerized aluminosilicate melts from ion dynamics simulations. Geochimica et Cosmochimica Acta, 55, 721–730.

Schairer, J.F., and Bowen, N.L. (1956) The system Na_2O-Al_2O_3-SiO_2. American Journal of Science, 254, 129–195.

Scherer, G.W. (1986) Relaxation in glass and composites, 331 p. Wiley, New York.

Seifert, F., Mysen, B.O., and Virgo, D. (1982) Three-dimensional network structure of quenched melts (glass) in the systems SiO_2-$NaAlO_2$, SiO_2-$CaAl_2O_4$ and SiO_2-$MgAl_2O_4$. American Mineralogist, 67, 696–717.

Sharma, S.K., Virgo, D., and Mysen, B. (1978) Structure of melts along the join SiO_2-$NaAlSiO_4$ by Raman spectroscopy. Carnegie Institution of Washington Year Book, 77, 652–658.

Shimizu, N., and Kushiro, I. (1984) Diffusivity of oxygen in jadeite and diopside melts at high pressures. Geochimica et Cosmochimica Acta, 48, 1295–1303.

Soules, T.F. (1979) A molecular dynamic calculation of the structure of sodium silicate glasses. Journal of Chemical Physics, 71, 4570–4578.

Soules, T.F., and Busbey, R.F. (1981) Sodium diffusion in alkali silicate glass by molecular dynamics. Journal of Chemical Physics, 75, 969–975.

Stebbins, J.F., and Sykes, D. (1990) The structure of $NaAlSi_3O_8$ liquid at high pressure: New constraints from NMR spectroscopy. American Mineralogist, 75, 943–946.

Stein, D.J. (1993) Aspects of momentum transport in magma: Experimental viscosity measurements and computer simulation studies, 147 p. Ph.D. dissertation, University of California, Santa Barbara, California.

Stein, D.J., and Spera, F.J. (1993) Experimental rheometry of melts and supercooled liquids in the system $NaAlSiO_4$-SiO_2: Implications for structure and dynamics. American Mineralogist, 78, 710–723.

Taylor, M., and Brown, G.E. (1979a) Structure of mineral glasses: I. The feldspar glasses $NaAlSi_3O_8$, $KAlSi_3O_8$, $CaAl_2Si_2O_8$. Geochimica et Cosmochimica Acta, 43, 61–75.

——— (1979b) Structure of mineral glasses: II. The SiO_2-$NaAlSiO_4$ join. Geochimica et Cosmochimica Acta, 43, 1467–1473.

Wasserman, E.A., Yuen, D.A., and Rustad, J.R. (1993a) Compositional effects on the transport and thermodynamic properties of MgO-SiO_2 mixtures using molecular dynamics. Physics of the Earth and Planetary Interiors, 77, 189–203.

——— (1993b) Molecular dynamics study of the transport properties of perovskite melts under high temperature and pressure conditions. Earth and Planetary Science Letters, 114, 373–384.

Wetherill, G.W. (1990) Formation of the Earth. Annual Review of Earth and Planetary Sciences, 18, 205–256.

Woodcock, L.V. (1975) Molecular dynamics calculations on molten ionic salts. In J. Braunstein, G. Mamantov, and G.P. Smith, Eds., Advances in molten salt chemistry, p. 1–74. Plenum, New York.

Woodcock, L.V., Angell, C.A., and Cheeseman, P. (1976) Molecular dynamics studies of the vitreous state: Simple ionic systems and silica. Journal of Chemical Physics, 65, 1565–1577.

Wright, A.C. (1993) The comparison of molecular dynamics simulations with diffraction experiments. Journal of Non-Crystalline Solids, 159, 264–268.

Zarzycki, J. (1991) Glasses and the vitreous state, 505 p. Cambridge University Press, New York.

Zirl, D.M., and Garofalini, S.H. (1990) Structure of sodium aluminosilicate glasses. Journal of the American Ceramic Society, 73, 2848–2856.